Quantum interference effects in topological nanowires in a longitudinal magnetic field

Vincent E. Sacksteder IV

W155 Wilson Building, Royal Holloway University of London, Egham Hill, Egham, TW20 0EX, United Kingdom

Quansheng Wu[*]

Theoretical Physics and Station Q Zurich, ETH Zurich, 8093 Zurich, Switzerland

We study the magnetoconductance of topological insulator nanowires in a longitudinal magnetic field, including Aharonov-Bohm, Altshuler-Aronov-Spivak, perfectly conducting channel, and universal conductance fluctuation effects. Our focus is on predicting experimental behavior in single wires in the quantum limit where temperature is reduced to zero. We show that changing the Fermi energy E_F can tune a wire from from ballistic to diffusive conduction and to localization. In both ballistic and diffusive single wires we find both Aharonov-Bohm and Altshuler-Aronov-Spivak oscillations with similar strengths, accompanied by quite strong universal conductance fluctuations, all with amplitudes between $0.3G_0$ and $1G_0$. This contrasts strongly with the average behavior of many wires, which shows Aharonov-Bohm oscillations in the ballistic regime and Altshuler-Aronov-Spivak oscillations in the diffusive regime, with both oscillations substantially larger than the conductance fluctuations. In single wires the ballistic and diffusive regimes can be distinguished by varying E_F and studying the sign of the Aharonov-Bohm signal, which depends periodically on E_F in ballistic wires and randomly on E_F in diffusive wires. We also show that in long wires the perfectly conducting channel is visible at a wide range of energies within the bulk gap. We present typical conductance profiles at several wire lengths, showing that conductance fluctuations can dominate the average signal. Similar behavior will be found in carbon nanotubes.

I. INTRODUCTION

Strong topological insulators (TIs) possess a band gap that can be used to eliminate electrical conduction through their interior, but unlike standard insulators they robustly host conducting surface states which completely wrap all of the TI sample's surfaces [1,2]. This unique circumstance allows realization of the celebrated Aharonov-Bohm effect, where electrons are sensitive to the total magnetic flux through a specific loop [3,4]. If a TI wire has a strictly constant cross section along the wire's length, and the surface state has strictly zero penetration into the interior, then the wire's conductance G will be a strictly periodic function of the magnetic flux Φ through the wire's cross section, i.e., $G(\Phi) = G(\Phi + \Phi_0)$, where $\Phi_0 = h/e$ is the magnetic flux quantum. This periodic dependence on the total magnetic flux threading the electron's path, and not on any local details of the path, is the hallmark of the Aharonov-Bohm (AB) effect.

A long string of experiments has realized the AB effect in TI wires, and has observed a zoo of periodic conductance features. One may distinguish between Aharonov-Bohm oscillations with period Φ_0 and Altshuler-Aronov-Spivak (AAS) oscillations with period $\Phi_0/2$ [5–23]. In addition, universal conductance fluctuations (UCFs) are observed—a noiselike component of $G(\Phi)$ which depends sensitively on the Fermi level and on disorder [5,9,24–30]. TIs also host a perfectly conducting channel (PCC)—a conductance quantum which is remarkable for its persistence in very long TI wires, its topological protection, and its status as a three-dimensional (3D) analog of the quantum Hall effect [17,31–42]. These effects are sensitive to the scattering length l, the localization length

L_{LOC}, the wire dimensions, Fermi level, and temperature. This rather complex experimental situation is accompanied by a vast theoretical literature [43–45] on mesoscopic conduction which with very few exceptions [39,41,42,46–48] predates topological insulators.

This paper offers an integrated view of these effects in the extreme quantum limit of zero temperature $T = 0$, where the AB effect is most visible and has the most remarkable consequences. This paper predicts the surface signal that experimentalists will see as they progressively implement improved TI devices with stronger quantum interference. If experiments eliminate bulk conduction, then only the surface signal described here will be observed; otherwise an additional bulk signal will be observed. We give special attention to the magnetoconductance's dependence on the Fermi level E_F because it can be controlled systematically via gating [49,50]. We also focus on single wires rather than the ensemble-averaged behavior of many wires, both because real experiments measure individual wires, and because ensemble averaging removes some of the most interesting aspects of the magnetoconductance. This focus contrasts with previous works using ensemble averages which showed that period Φ_0 AB oscillations are dominant in ballistic wires smaller than the scattering length l and period $\Phi_0/2$ AAS oscillations are dominant in diffusive wires larger than l [46,47]. In contrast, we show that single wires at $T = 0$ manifest significant AB and AAS oscillations, as well as universal conduction fluctuations of the same or larger amplitude, regardless of whether they are ballistic or diffusive.

II. THE MODEL

We study TI nanowires fulfilling all the conditions necessary to ensure that the conductance be perfectly periodic

---

[*]wuquansheng@gmail.com

throughout most of the bulk gap. Briefly, these conditions are the following: a uniform cross section, negligible penetration of the surface state into the bulk, a perfectly parallel magnetic field, and the absence of bulk conduction. Any nonperiodic component of the conductance implies violation of one of these conditions. In particular, violation of the first three conditions generically has the same result: the periodic signal remains unchanged at small magnetic fluxes, but is extinguished once the flux exceeds a threshold $N\Phi_0$. The coefficient N is infinite in an ideal TI wire and decreases as the wire quality worsens. In Appendix B we give simple estimates of N. Based on these estimates, we expect that as long as the penetration depth and wire nonuniformity are less than a tenth of the wire radius, and the magnetic field is aligned with the wire axis within a tenth of a radian, $N \geqslant 5$ and the conductance should exhibit at least five Φ_0 periods on either side of $B = 0$ before being extinguished. In particular, in the Bi_2Se_3 family of TIs which display a penetration depth $\lambda = 2$–3 nm, the wire radius should be of order 20 nm [51]. This is, in fact, the length scale chosen in many previous experiments on TI wires [5].

Violation of the last condition, the absence of bulk conduction, has much different effects. Generically, bulk conduction will cause additional features in the conductance which are not periodic in the flux with period Φ_0, so that the periodic surface signal of interest can be studied only after filtering out the nonperiodic signals. The most notable such feature is an additional weak antilocalization conductance peak centered at zero flux, which has been reported in most experimental measurements of AB oscillations in TI wires. In addition, in long wires bulk conduction will cause the topological surface state to tunnel through the bulk and be destroyed [38]. Two other frequently observed signatures of bulk conduction are a noiselike dependence on Φ which is slower than Φ_0, and an overall parabolic trend seen over many multiples of Φ_0. Further discussion of these effects is outside the scope of this paper.

We use a computationally efficient minimal tight-binding model of a strong $\mathbb{Z}_2$ TI implemented on a cubic lattice. With four orbitals per site, the model's momentum representation is

$$H = \sum_{i=1}^{3} \left[\left(i\frac{t}{2}\alpha_i - \frac{1}{2}\beta \right) e^{-ik_i a} + \text{H.c.} \right] + (m+3)\beta. \quad (1)$$

$\alpha_i = \sigma_x \otimes \sigma_i$ and $\beta = \sigma_z \otimes 1$ are gamma matrices in the Dirac representation, $t = 2$ is the hopping strength, $m = -1$ is the mass parameter, and $a = 1$ is the lattice spacing [52–55]. The large bulk band gap $E = [-1, 1]$ ensures that the surface state's penetration depth is very small, of order $O(a)$. Our wires have constant height and width $h = w = 10$, which is large enough to ensure that the topological state does not decay via tunneling through the bulk of the wire [38].

To model scattering effects we add uncorrelated white noise disorder $u(x)$ chosen randomly from the interval $[-W/2, W/2]$, where $W = 2$ is the disorder strength. The disorder is located only on the TI sample's outer surface, and has a depth of one lattice unit. Our numerical studies have shown that as long as the Fermi level is not near the edges of bulk gap this disorder's qualitative and quantitative effects on the topological state are weak: the state remains tightly pinned to the surface and exhibits a fairly uniform surface
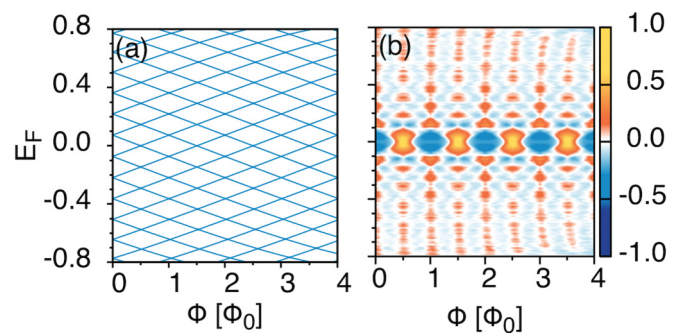

FIG. 1. The Aharonov-Bohm effect in 10×10 wires. Pane (a) shows the surface state's spectrum in clean wires. Pane (b) shows the ensemble average of the magnetoconductance $G(E_F, \Phi)$ in $L_x = 67$ wires, with the average over Φ subtracted out. The regime of ballistic conduction is visible in the interval $E_{\text{gap}} < |E_F| < E_l$, where a cross-hatched pattern matches pane (a). At larger energies $E_l < |E_F|$ the vertical stripes show diffusive conduction. Near the Dirac point $|E_F| < E_{\text{gap}}$ a small gap induced by spin-momentum locking causes localization. $E_{\text{gap}} = 0.07$ is the maximal height of the gap reached at integer values of the magnetic flux, and $E_l = 0.35$ is the energy where the scattering length l becomes smaller than the wire dimensions.

density similar to that of a plane wave [38,56]. Moreover its density of states, Fermi velocity, etc., do not undergo large changes. Our choice of weak surface disorder and no bulk disorder eliminates bulk conduction and minimizes the penetration depth so that the AB effect is optimally realized. In real experiments with bulk disorder, as long as the Fermi level is not near the edges of the band gap, and as long as the disorder does not introduce carriers in the bulk of the wire, the disorder's main effect will be a mild renormalization of the penetration depth. It will not cause qualitative differences from the results presented here.

To calculate the conductance we use the Caroli formula $G = -G_0 \text{Tr}[(\Sigma_L^r - \Sigma_L^a)G_{LR}^r(\Sigma_R^r - \Sigma_R^a)G_{RL}^a]$ [57,58]. $G_0 = e^2/h$ is the conductance quantum, $\eta = 10^{-9}$ regularizes the calculation, $G^a, G^r = (E_F - H - u \mp \iota\epsilon)^{-1}$ are the advanced and retarded single-particle Green's functions connecting the left and right leads, and $\Sigma_{L,R}$ are the lead self-energies. For leads we minimize the contact resistance by using perfectly conducting one-dimensional (1D) wires connected to each site on the sample's ends, i.e., at the two ends of the wire each orbital on each site is connected to a semi-infinite 1D chain. The self-energy Γ is simply $(2t)^{-1}\exp(i\phi)$, where t is the hopping strength within the leads and ϕ encodes the Fermi level [59,60].

III. CONTROL OF CONDUCTION BY CHANGING THE FERMI ENERGY

In a 3D TI the scattering length l varies inversely with the Fermi energy. Therefore a single TI wire can be ballistic, i.e., smaller than the scattering length, at a small value of E_F, and at the same time diffusive, i.e., larger than the scattering length, at a larger E_F. Figure 1(b) highlights the ballistic and the diffusive regimes in TI wires of length $L = 67$. It shows the ensemble-averaged magnetoconductance

$G(E_F, \Phi)$, which is known to be dominated by period Φ_0 AB oscillations in the ballistic regime. The *ballistic* regime is visible as a clear cross-hatched pattern in the energy range $E_{\text{gap}} < |E_F| < E_l$, with $E_{\text{gap}} = 0.07$, $E_l = 0.35$. This pattern is caused directly by the cross-hatched energy dispersion of the clean wire, shown in Fig. 1(a). At $|E_F| = E_l$ the scattering length l becomes smaller than the wire dimensions, and the wires become *diffusive*. We show in Appendix A that $l \propto v_F^3/W^2\xi^2 E_F$, where $v_F = 2$ is the Fermi velocity, W is the disorder strength, and ξ is the disorder correlation length. In individual wires the value of the energy E_l separating the diffusive and ballistic regimes depends sensitively on the scattering length l, which is determined by the impurity type and concentration and requires experimental measurement on a case by case basis. One way of determining l is by placing leads at several distances along the wire length and measuring several resistances, and another is by measuring the Hall resistance [61]. In our wires l is equal to the perimeter P when $|E_F| = E_l = 0.35$. Above this energy our wires are diffusive, so the ballistic cross-hatched pattern in Fig. 1(b) is replaced by vertical stripes spaced at intervals of $\Phi_0/2$—the well known AAS oscillations.

Figure 1(b) shows much different physics near the Dirac point, at $|E_F| < E_{\text{gap}}$. Here the conductance is never more than $G = 1G_0$, putting the sample in the *localized* regime where quantum-mechanical interference controls conduction. When the flux has half-integer values $\Phi = (n + 1/2)\Phi_0$ the perfectly conducting channel is visible—a single conductance quantum $G = 1G_0$ which is topologically protected. At other values of the flux the TI's locking between spin and momentum, combined with the wire's finite size, opens a small gap around the Dirac point, causing the conductance to decrease exponentially with wire length. The gap reaches its maximum height $E_{\text{gap}} = \sqrt{2}\, v_F/P \approx 0.07$ at integer flux $\Phi = n\,\Phi_0$, where $P = 40$ is the wire's perimeter. In a 50 nm × 50 nm Bi$_2$Se$_3$ wire, $E_{\text{gap}} \approx 14$ meV, about one-twentieth of the bulk band gap.

At energies E_F outside the gap, i.e., $|E_F| > E_{\text{gap}}$ in our samples, the localization length $L_{\text{LOC}} \propto l\,|E_F|/E_{\text{gap}}$. In individual wires L_{LOC} will have to be determined on a case by case basis. Because l varies inversely with the Fermi energy E_F, the localization length $L_{\text{LOC}} \propto v_F^2\, P\,/W^2\xi^2$ is independent of E_F (see Appendix A for a derivation). The only way to enter the localized regime, other than tuning E_F near the Dirac point, is to lengthen or narrow the wire, or increase the disorder.

IV. SINGLE WIRES

Figure 2(a) presents the magnetoconductance $G(E_F, \Phi)$ of a single $L = 67$ wire. The single-wire data manifests the same localized, ballistic, and diffusive regimes that are so clear in the ensemble-averaged $L = 67$ wires presented earlier. It is, however, much more rich and detailed than the ensemble average, so we present the Fourier transform $G(E_F, \Omega)$ of the conductance in Fig. 2(b), which affords a more precise analysis. The Fourier transform is peaked at integer frequencies $\Omega = 1/\Phi_0, 2/\Phi_0, 3/\Phi_0, \ldots$ and zero elsewhere, resulting in the vertical lines seen in pane (b). The vertical
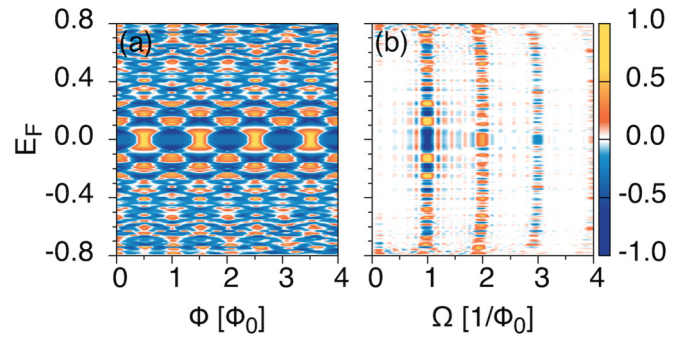

FIG. 2. A single $L = 67$ wire showing ballistic conduction at $E_{\text{gap}} < |E_F| < E_l$, diffusive conduction at $E_l < |E_F|$, and localization at $|E_F| < E_{\text{gap}}$. The left pane shows the magnetoconductance $G(E_F, \Phi)$, and the right pane shows its Fourier transform $G(E_F, \Omega)$. The average over Φ has been removed. $E_{\text{gap}} = 0.07$ is the height of the gap, and $E_l = 0.35$ is the energy where the scattering length l becomes smaller than the wire dimensions.

line at $\Omega = 1/\Phi_0$ shows AB oscillations, while the line at $\Omega = 2/\Phi_0$ shows AAS oscillations.

Figure 2(b) shows that in single wires at $T = 0$, as opposed to ensembles of wires, AB oscillations cannot be taken as a sign of ballistic conduction, and AAS oscillations are not a sign of diffusive conduction. We find AB and AAS signals both in the ballistic regime at $|E_F| < E_l$ and in the diffusive regime at $|E_F| > E_l$. In the ballistic regime the AB amplitude oscillates periodically as a function of E_F in the range $[-\,G_0, +\,G_0]$, producing the cross-hatched pattern in Fig. 2(a). In the diffusive regime the AB signal depends randomly on E_F and generally remains in the range $[-0.4, 0.4]G_0$. In both the ballistic and diffusive regimes the AAS signal amplitude is a random function of E_F, and generally less than $0.4G_0$. We conclude that in single wires at $T = 0$ the presence or absence of AB and AAS signals cannot be used to determine whether conduction is ballistic or diffusive. The only way to determine this is to systematically vary the Fermi level E_F and determine whether the AB amplitude is a periodic function of E_F as in the ballistic regime or instead random as in the diffusive regime.

Our finding of AB oscillations in the diffusive regime confirms and extends a recent experiment which found an AB signal in quite long wires as long as the perimeter $P < l$ is less than than the scattering length l [18]. We find that if $P < l$ the AB signal depends periodically on E_F, and if $P > l$ its amplitude is random. Our observation of AAS oscillations verifies theoretical work showing that they occur in the ballistic regime as a consequence of constructive quantum interference between time-reversed circuits around the wire [62–65].

The Fourier transform in Fig. 2(b) also shows that the AAS signal is predominantly positive across all values of the Fermi energy. In Fig. 2(a) this means that the pattern of vertical AAS stripes has its maxima at half integer flux $\Phi = 0, \Phi_0/2, \Phi_0, 3\Phi_0/2, \ldots$ and minima at quarter flux. These minima and maxima are interchanged, and the Fourier transform's AAS signal is negative, in materials displaying weak localization. The positive AAS signal seen in TIs is a direct indicator of weak antilocalization.

Comparison of the single-wire data in Fig. 2 to the averaged data in Fig. 1(b) shows that universal conductance fluctuations,

noiselike deviations of single wires from the ensemble average, pervade both the ballistic and diffusive regimes. They occur at the AB and AAS frequencies, and also at higher frequencies. In our $T = 0$ single wires the UCF magnitude is 0.2–0.35G_0, so UCFs account for much of the total dependence on Φ in single wires, including the entire AB signal seen in the diffusive regime. It is particularly remarkable that we find UCFs in the ballistic regime, where most (but not all) of the electrons transiting the length of the wire do not scatter. A single scattered electron is enough to change the conductance by 1G_0.

These results are expected to change with temperature. Broadly speaking, the effect of temperature is to reduce the total variation in $G(\Phi)$ and to remove frequencies in $G(\Omega)$, generally resulting in a smoother signal. Although AB oscillations of order 1G_0 have been observed in two experiments [9,21], often a second scenario is observed where the measured signal is a small fraction of G_0 [17,19,22], and very often only the AB signal is found. Finite temperatures can cause this scenario, regardless of whether the sample is ballistic or diffusive, by introducing a dephasing length L_ϕ beyond which quantum effects are extinguished by inelastic scattering. L_ϕ depends sensitively on both temperature and scattering, and in TIs has been measured to have values from 100 nm to microns [9,28,61]. If the dephasing length L_ϕ is smaller than the perimeter P the magnetoconductance is exponentially suppressed, with the Nth frequency $\Omega = N/\Phi_0$ controlled by $\exp(-NL_\phi/P)$ [4,9,17,22]. A small value of $L_\phi/P < 1$ can explain experiments where the total variation in $G(\Phi)$, in units of conductance, is substantially less than 1G_0, and the AAS signal is weak or absent. In such experiments the AB signal should decrease exponentially with temperature, both in the ballistic and in the diffusive regime.

If, on the other hand, the inelastic dephasing length L_ϕ exceeds the wire perimeter, then the principal effect of temperature is via a second mechanism, smearing of the Fermi energy E_F over the thermal width $k_B T$. This thermal broadening can cause a substantial reduction in the AB signal, whose sign is sensitive to E_F, while leaving the AAS signal relatively unscathed. In diffusive wires with weak inelastic dephasing, thermal broadening is expected to cause the AB signal to scale with $1/\sqrt{T}$, which has been confirmed by several experiments [5–7,10,11,20,66,67].

V. LONG WIRES AND THE PERFECTLY CONDUCTING CHANNEL

Figure 3 shows a single long wire in the localized regime, which hosts a PCC. The PCC manifests as spectacular very narrow vertical stripes with unit conductance extending through the bulk gap and almost reaching the bulk band, so in long wires there is no need to tune the Fermi energy to find the PCC. The quantized conductance repeats at half-integer flux $\Phi = (n + 1/2)\Phi_0$. At other values of Φ the conductance decays exponentially with wire length as is typical in localized wires, so the PCC stripes are very narrow. This ensures that many frequencies are present in the Fourier transform [Fig. 3(b)], and that the even frequencies $\Omega = 0, 2/\Phi_0, 4/\Phi_0, \ldots$ have negative sign while the odd frequencies $\Omega = \Phi_0, 3/\Phi_0, \ldots$ have positive sign. The peak sharpness, and also the number of
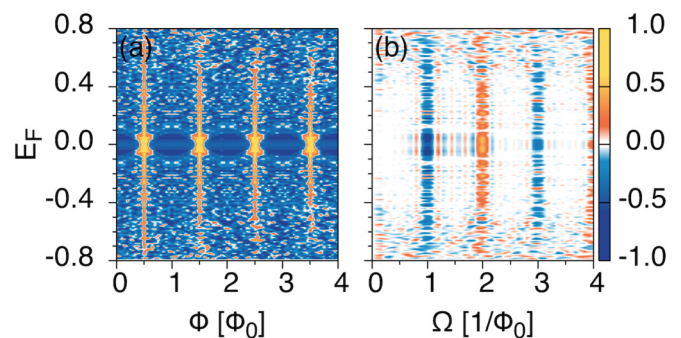

FIG. 3. A single long $L = 403$ wire in the localized regime, showing the perfectly conducting channel at $\Phi = \Phi_0/2, 3\Phi_0/2, 5\Phi_0/2, \ldots$. The left pane shows the magnetoconductance $G(E_F, \Phi)$, and the right pane shows its Fourier transform $G(E_F, \Omega)$. The average over Φ has been removed. The localization length is $L_{\mathrm{LOC}} \approx 200$.

frequencies in the Fourier transform, increases with the wire length. The quantization of the PCC peaks is controlled by their magnetic-flux-induced decay length, which far exceeds the localization length and scales with the cube of the wire width w^3 [38].

As discussed earlier and shown in Fig. 2, the PCC can be observed in short wires near the Dirac point. However, in this case the PCC peaks are roughly sinusoidal and match well with a basic AB signal.

To our knowledge, in 3D TIs the PCC's sensitivity to temperature has not yet been studied. Graphene ribbons with zigzag edges exhibit a pair of PCCs, one for each of graphene's two valleys, resulting in a 2G_0 conductance. These PCCs are known to be unstable against dephasing via a mechanism which mixes the two valleys [33,40]. We emphasize here that the PCC in 3D TIs is not vulnerable to the same decay mechanism, because there is an odd number of conducting channels and a single PCC [41,42]. In particular, dephasing per se, i.e., randomization of the wave function's phase, can affect only short wires where the conductance is larger than 1G_0. In these samples such dephasing will eliminate weak antilocalization, which in the absence of dephasing multiplies the conductance by $\ln L/l$. Here L is the sample size and l is the scattering length. In longer wires where only the PCC remains and the conductance is quantized at 1G_0, dephasing per se cannot produce any further effect on the single remaining channel [37,40,68]. However, unlike a truly one-channel topological wire, the surfaces of quasi-one-dimensional 3D TI wires do host localized states. There is some possibility that inelastic many-body processes might be able to couple those states to the PCC and eventually destroy the PCC. Further study of this possibility would require a careful perturbative treatment of interactions similar to the analysis applied to two-dimensional (2D) TI edge states in Refs. [69,70], combined with careful numerical analysis of both localized and PCC states in long TI wires. Such analysis is outside the scope of the present paper.

Figure 4 summarizes typical magnetoconductance profiles at fixed E_F and zero temperature in ultrashort (yellow), ballistic (red), diffusive (blue), and localized (purple) wires. Single-wire results are shown in bold, and the ensemble
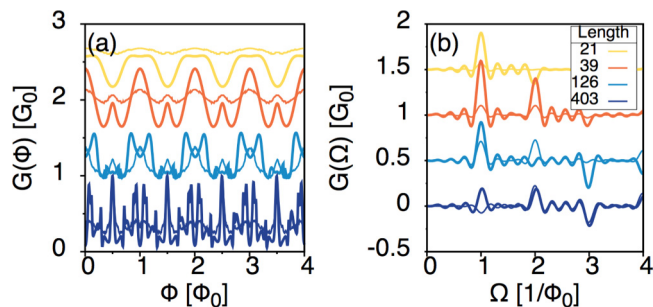
FIG. 4. Magnetoconductance $G(\Phi)$ and its Fourier transform $G(\Omega)$ at four wire lengths corresponding to ultrashort, ballistic, diffusive, and localized wires. Thick lines show the conductance of a single wire and thin lines show the ensemble average. The fast Fourier transform lines have been shifted to allow comparison and the $\Omega = 0$ component has been removed. $E_F = 0.26$ and the scattering and localization lengths are $l \approx 50$, $L_{\mathrm{LOC}} \approx 200$.

average is shown with thin lines. The AB oscillations seen in the ensemble average of the diffusive (blue) wires are caused by the perimeter P being less than the scattering length l, and will disappear in the opposite case of $P > l$. At each of the four wire lengths the UCF strength, i.e., the standard deviation of $G(\Phi)$, is 0.2–0.35G_0. In ultrashort and ballistic wires the max vs min of the ensemble average is 0.08G_0 and 0.18G_0, respectively, which is small compared to the UCFs. Therefore in single wires at fixed E_F the amplitude of the AB and AAS signals has a very strong random component. In diffusive and localized wires the ensemble max vs min grows to 0.42G_0 and 0.75G_0, so that single-wire results get closer to the average behavior, albeit with still strong randomness. In particular, single localized wires should reliably manifest a picket fence pattern of PCC peaks.

Lastly we point out that the longitudinal magnetoconductance of carbon nanotubes [71,72] is quite similar to that of the TI wires studied here, with only three differences.

First, carbon nanotubes exhibit four species of Dirac particles, in two valleys and with two distinct spins, multiplying the ballistic conductance and the PCC by four. Second, the perfectly conducting channel occurs at integer flux, not half-integer flux; no magnetic field is required to see the PCC in carbon nanotubes. Third, if short range scattering or interactions mix the two graphene valleys, then the valley mixing will kill the PCC and reverse the sign of the AAS signal. Aside from these details, the magnetoconductance should be similar to that of TI wires, including the relative strength of the various effects.

APPENDIX A: THE SCATTERING AND LOCALIZATION LENGTHS

The scattering length l can be obtained from the self-consistent Born approximation $\hbar/\tau = \gamma\rho$, where τ is the scattering time, γ is the scattering strength, and ρ is the density of states. The topological surface state obeys a 2D Dirac dispersion, resulting in a density of states $\rho \propto E_F/v_F^2$ which is proportional to the Fermi energy E_F, where v_F is the Fermi velocity. The scattering time τ is related to the scattering length l by $\tau = l/v_F$. Using $\gamma \propto W^2\xi^2$, where W is the disorder strength and ξ is the disorder correlation length, and setting $\hbar = 1$, we obtain the scattering length formula given in the text, $l \propto v_F^3/W^2\xi^2 E_F$.

The localization length L_{LOC} can be estimated from $L_{\mathrm{LOC}} \propto l N$, where $N \propto |E_F|/E_{\mathrm{gap}}$ is the number of conducting channels in a clean wire. In a 2D electron gas of width w the number of conducting channels is $N \propto w\rho v_F$. On the surface of a TI wire w is equal to the wire perimeter P. Using again $\rho \propto E_F/v_F^2$, we obtain the localization length formula given in the text, $L_{\mathrm{LOC}} \propto v_F^2 P/W^2\xi^2$.

APPENDIX B: EFFECTS OF NONIDEAL NANOWIRES ON THE AB EFFECT

We consider the effect of a nonuniform wire cross section, penetration of the surface state into the bulk, and the presence of a magnetic field component perpendicular to the axis of the TI wire. Each of these three effects add an additional length scale λ to the wire:

(1) Nonuniform cross section: For each cross section A we can calculate an effective radius $r = \sqrt{A/\pi}$. The new length scale λ is the difference between r's minimum and maximum values, i.e., $\lambda = r_{\mathrm{max}} - r_{\mathrm{min}}$.

(2) Penetration into the bulk: Here λ is the penetration depth [4].

(3) Perpendicular magnetic field: In this case λ is the radius r of the wire multiplied by the sine of the angle of the total magnetic field with respect to the wire axis, i.e., $\lambda = r \sin\theta$. [4]

In ideal wires λ is zero. Assuming that the wire is not too far from perfection, i.e., λ is small compared to the wire radius, we calculate the magnetic flux Φ_λ through the portion of the wire which is affected by the wire imperfection. The cross section of this imperfect part is $2\pi r\lambda$. Assuming that the wire's total cross section is πr^2, and that a total flux Φ passes through the cross section of the wire, we find that $\Phi_\lambda = (2\lambda/r)\Phi$ flux units pass through the imperfect part of the wire.

It is the Φ_λ flux which is sensitive to the wire's imperfections, and which multiplies the signal by a random phase $\exp(i\Phi_\lambda/\Phi_0)$. As long as the phase is small, i.e., $\Phi_\lambda < \Phi_0$ is less than one flux quantum, the imperfection has little effect. However, once Φ_λ exceeds one flux quantum, the imperfection is able to completely randomize the phase and destroy the Aharonov-Bohm effect. Therefore we identify the threshold value of the total magnetic flux as $N\Phi_0$, where $N = r/2\lambda$, r is the wire radius, and λ is given above. In particular, when the magnetic field is not perfectly parallel to the TI wire, $N = (2\sin\theta)^{-1}$. The first N periodic oscillations of the conductance will be easily visible in the experimental data, while higher oscillations will be extinguished.

[1] H. Zhang, C.-X. Liu, X.-L. Qi, X. Dai, Z. Fang, and S.-C. Zhang, Nat. Phys. **5**, 438 (2009).

[2] M. Z. Hasan and C. L. Kane, Rev. Mod. Phys. **82**, 3045 (2010).

[3] Y. Aharonov and D. Bohm, Phys. Rev. **115**, 485 (1959).

[4] A. G. Aronov and Y. V. Sharvin, Rev. Mod. Phys. **59**, 755 (1987).

[5] H. Peng, K. Lai, D. Kong, S. Meister, Y. Chen, X.-L. Qi, S.-C. Zhang, Z.-X. Shen, and Y. Cui, Nat. Mater. **9**, 225 (2010).

[6] F. Xiu, L. He, Y. Wang, L. Cheng, L.-T. Chang, M. Lang, G. Huang, X. Kou, Y. Zhou, X. Jiang *et al.*, Nat. Nanotechnol. **6**, 216 (2011).

[7] S. Lee, J. In, Y. Yoo, Y. Jo, Y. C. Park, H.-J. Kim, H. C. Koo, J. Kim, B. Kim, and K. L. Wang, Nano Lett. **12**, 4194 (2012).

[8] Z. Li, Y. Qin, F. Song, Q.-H. Wang, X. Wang, B. Wang, H. Ding, C. Van Haesondonck, J. Wan, Y. Zhang *et al.*, Appl. Phys. Lett. **100**, 083107 (2012).

[9] J. Dufouleur, L. Veyrat, A. Teichgräber, S. Neuhaus, C. Nowka, S. Hampel, J. Cayssol, J. Schumann, B. Eichler, O. G. Schmidt *et al.*, Phys. Rev. Lett. **110**, 186806 (2013).

[10] A. Sulaev, P. Ren, B. Xia, Q. H. Lin, T. Yu, C. Qiu, S.-Y. Zhang, M.-Y. Han, Z. P. Li, W. G. Zhu *et al.*, AIP Adv. **3**, 032123 (2013).

[11] B. Hamdou, J. Gooth, A. Dorn, E. Pippel, and K. Nielsch, Appl. Phys. Lett. **102**, 223110 (2013).

[12] M. Tian, W. Ning, Z. Qu, H. Du, J. Wang, and Y. Zhang, Sci. Rep. **3**, 1212 (2013).

[13] B. Hamdou, J. Gooth, A. Dorn, E. Pippel, and K. Nielsch, Appl. Phys. Lett. **103**, 193107 (2013).

[14] M. Safdar, Q. Wang, M. Mirza, Z. Wang, K. Xu, and J. He, Nano Lett. **13**, 5344 (2013).

[15] H. Zhu, E. Zhao, C. A. Richter, and Q. Li, ECS Trans. **64**, 51 (2014).

[16] K. Zhu, L. Wu, X. Gong, S. Xiao, S. Li, X. Jin, M. Yao, D. Qian, M. Wu, J. Feng *et al.*, arXiv:1403.0066.

[17] S. S. Hong, Y. Zhang, J. J. Cha, X.-L. Qi, and Y. Cui, Nano Lett. **14**, 2815 (2014).

[18] J. Dufouleur, L. Veyrat, E. Xypakis, J. H. Bardarson, C. Nowka, S. Hampel, B. Eichler, O. G. Schmidt, B. Büchner, and R. Giraud, arXiv:1504.08030.

[19] L. A. Jauregui, M. T. Pettes, L. P. Rokhinson, L. Shi, and Y. P. Chen, Nat. Nanotechnol. **11**, 345 (2016).

[20] L. A. Jauregui, M. T. Pettes, L. P. Rokhinson, L. Shi, and Y. P. Chen, Sci. Rep. **5**, 8452 (2015).

[21] S. Cho, B. Dellabetta, R. Zhong, J. Schneeloch, T. Liu, G. Gu, M. J. Gilbert, and N. Mason, Nat. Commun. **6**, 7634 (2015).

[22] H.-S. Kim, H. S. Shin, J. S. Lee, C. W. Ahn, J. Y. Song, and Y.-J. Doh, Curr. Appl. Phys. **16**, 51 (2016).

[23] J. Kim, A. Hwang, S.-H. Lee, S.-H. Jhi, S. Lee, Y. C. Park, S.-i. Kim, H.-S. Kim, Y.-J. Doh, J. Kim *et al.*, ACS Nano **10**, 3936 (2016).

[24] J. G. Checkelsky, Y. S. Hor, R. J. Cava, and N. P. Ong, Phys. Rev. Lett. **106**, 196801 (2011).

[25] S. Matsuo, T. Koyama, K. Shimamura, T. Arakawa, Y. Nishihara, D. Chiba, K. Kobayashi, T. Ono, C.-Z. Chang, K. He *et al.*, Phys. Rev. B **85**, 075440 (2012).

[26] S. Matsuo, K. Chida, D. Chiba, T. Ono, K. Slevin, K. Kobayashi, T. Ohtsuki, C.-Z. Chang, K. He, X.-C. Ma *et al.*, Phys. Rev. B **88**, 155438 (2013).

[27] B. Zhao, T. Chen, H. Pan, F. Fei, and Y. Han, J. Phys.: Condens. Matter **27**, 465302 (2015).

[28] B. Xia, P. Ren, A. Sulaev, P. Liu, S.-Q. Shen, and L. Wang, Phys. Rev. B **87**, 085442 (2013).

[29] Z. Li, Y. Meng, J. Pan, T. Chen, X. Hong, S. Li, X. Wang, F. Song, and B. Wang, Appl. Phys. Express **7**, 065202 (2014).

[30] J. Kim, S. Lee, Y. M. Brovman, M. Kim, P. Kim, and W. Lee, Appl. Phys. Lett. **104**, 043105 (2014).

[31] M. R. Zirnbauer, Phys. Rev. Lett. **69**, 1584 (1992).

[32] A. D. Mirlin, A. Muller-Groeling, and M. R. Zirnbauer, Ann. Phys. (NY) **236**, 325 (1994).

[33] T. Ando and H. Suzuura, J. Phys. Soc. Jpn. **71**, 2753 (2002).

[34] Y. Takane, J. Phys. Soc. Jpn. **73**, 1430 (2004).

[35] S. Ryu, C. Mudry, H. Obuse, and A. Furusaki, Phys. Rev. Lett. **99**, 116601 (2007).

[36] K. Wakabayashi, Y. Takane, and M. Sigrist, Phys. Rev. Lett. **99**, 036601 (2007).

[37] Y. Ashitani, K.-I. Imura, and Y. Takane, in *International Journal of Modern Physics: Conference Series* (World Scientific, Singapore, 2012), Vol. 11, pp. 157–162.

[38] Q. Wu and V. E. Sacksteder, Phys. Rev. B **90**, 045408 (2014).

[39] E. B. Kolomeisky and J. P. Straley, arXiv:1409.7974.

[40] Y. Shimomura and Y. Takane, J. Phys. Soc. Jpn. **85**, 014704 (2015).

[41] Y. Zhang and A. Vishwanath, Phys. Rev. Lett. **105**, 206601 (2010).

[42] R. Egger, A. Zazunov, and A. L. Yeyati, Phys. Rev. Lett. **105**, 136403 (2010).

[43] P. A. Lee and T. V. Ramakrishnan, Rev. Mod. Phys. **57**, 287 (1985).

[44] J. Rammer and H. Smith, Rev. Mod. Phys. **58**, 323 (1986).

[45] C. W. J. Beenakker, Rev. Mod. Phys. **69**, 731 (1997).

[46] J. H. Bardarson, P. W. Brouwer, and J. E. Moore, Phys. Rev. Lett. **105**, 156803 (2010).

[47] J. H. Bardarson and J. E. Moore, Rep. Prog. Phys. **76**, 056501 (2013).

[48] P. Adroguer, D. Carpentier, J. Cayssol, and E. Orignac, New J. Phys. **14**, 103027 (2012).

[49] J. Chen, H. J. Qin, F. Yang, J. Liu, T. Guan, F. M. Qu, G. H. Zhang, J. R. Shi, X. C. Xie, C. L. Yang *et al.*, Phys. Rev. Lett. **105**, 176602 (2010).

[50] Y. Wen-Min, L. Chao-Jing, L. Jian, and L. Yong-Qing, Chin. Phys. B **22**, 097202 (2013).

[51] W. Zhang, R. Yu, H.-J. Zhang, X. Dai, and Z. Fang, New J. Phys. **12**, 065013 (2010).

[52] C.-X. Liu, X.-L. Qi, H. J. Zhang, X. Dai, Z. Fang, and S.-C. Zhang, Phys. Rev. B **82**, 045122 (2010).

[53] S. Ryu and K. Nomura, Phys. Rev. B **85**, 155138 (2012).

[54] K. Kobayashi, T. Ohtsuki, and K.-I. Imura, Phys. Rev. Lett. **110**, 236803 (2013).

[55] K. Kobayashi, T. Ohtsuki, K.-I. Imura, and I. F. Herbut, Phys. Rev. Lett. **112**, 016402 (2014).

[56] V. Sacksteder, T. Ohtsuki, and K. Kobayashi, Phys. Rev. Appl. **3**, 064006 (2015).

[57] C. Caroli, R. Combescot, P. Nozieres, and D. Saint-James, J. Phys. C **4**, 916 (1971).

[58] Y. Meir and N. S. Wingreen, Phys. Rev. Lett. **68**, 2512 (1992).

[59] M. P. L. Sancho, J. M. L. Sancho, and J. Rubio, J. Phys. F **15**, 851 (1985).

[60] C. H. Lewenkopf and E. R. Mucciolo, J. Comput. Electron. **12**, 203 (2013).

[61] C. J. Lin, X. Y. He, J. Liao, X. X. Wang, V. S. IV, W. M. Yang, T. Guan, Q. M. Zhang, L. Gu, G. Y. Zhang *et al.*, Phys. Rev. B **88**, 041307 (2013).

[62] S. Kawabata and K. Nakamura, J. Phys. Soc. Jpn. **65**, 3708 (1996).

[63] S. Kawabata and K. Nakamura, Phys. Rev. B **57**, 6282 (1998).

[64] C.-K. Lee, J. Cho, J. Ihm, and K.-H. Ahn, Phys. Rev. B **69**, 205403 (2004).

[65] T. Koga, J. Nitta, and M. van Veenhuizen, Phys. Rev. B **70**, 161302 (2004).

[66] S. Washburn, C. P. Umbach, R. B. Laibowitz, and R. A. Webb, Phys. Rev. B **32**, 4789 (1985).

[67] A. E. Hansen, A. Kristensen, S. Pedersen, C. B. Sørensen, and P. E. Lindelof, Phys. Rev. B **64**, 045327 (2001).

[68] Y. Takane, J. Phys. Soc. Jpn. **79**, 024711 (2010).

[69] T. L. Schmidt, S. Rachel, F. von Oppen, and L. I. Glazman, Phys. Rev. Lett. **108**, 156402 (2012).

[70] N. Kainaris, I. V. Gornyi, S. T. Carr, and A. D. Mirlin, Phys. Rev. B **90**, 075118 (2014).

[71] C. Strunk, B. Stojetz, and S. Roche, Semicond. Sci. Technol. **21**, S38 (2006).

[72] B. Stojetz, S. Roche, C. Miko, F. Triozon, L. Forro, and C. Strunk, New J. Phys. **9**, 56 (2007).